ATOMISTIC STUDIES OF PROPERTIES OF HELIUM IN BCC IRON USING THE NEW HE–FE POTENTIAL—David M. Stewart, Stanislav Golubov (Oak Ridge National Laboratory and the University of Tennessee), Yuri Ostesky, Roger E. Stoller, Tatiana Seletskaia, and Paul Kamenski (Oak Ridge National Laboratory)

SUMMARY

In fusion applications, helium caused by transmutation plays an important role in the response of RAFM steels to neutron radiation damage. The growth, migration and coalescence behavior of helium bubbles is very sensitive to the properties of individual He interstitials and helium-vacancy clusters [1]. We have performed atomistic simulations using a new 3-body Fe–He inter-atomic potential [2–4] combined with the Ackland [5] iron potential. With the ORNL potential, interstitial helium is very mobile and coalesces together to form interstitial clusters. The interstitial clusters show lower binding energy than with the Wilson potential [6], in agreement with the DFT calculations of CC Fu [7]. If the He cluster is sufficiently large the cluster can push out an Fe interstitial, creating a Frenkel pair. The resulting helium-vacancy cluster is not mobile. The ejected SIA is mobile, but is weakly trapped by the He-V cluster. If more helium atoms join the He-V cluster, more Fe interstitials can be pushed out, and they combine to form an interstitial dislocation loop. Such loops have been observed in experiment—for example in [8]. The reverse process is also studied. Multiple helium atoms can be trapped in a single vacancy, and if there are few enough, the vacancy can recombine with an Fe interstitial to create a helium interstitial cluster.

PROGRESS AND STATUS

Introduction

Helium produced in neutron irradiated iron plays an important part in its mechanical properties. A new He–Fe inter-atomic potential has been developed at ORNL, based on extensive fitting to first-principles calculations of point defects and clusters [2–4]. This potential has been used to investigate the properties of helium and helium-vacancy clusters in MD and MS simulations.

Potential

The ORNL 3-body potential is described in [2] and [3] and [4]. The potential was fitted to first principles calculations done in VASP. Fitted configurations included relaxed and unrelaxed defects, so that forces could be fitted as well as energies. A key result from the DFT calculations is that the tetrahedral interstitial site is more stable than the octahedral site. Reproducing this feature is difficult as the octahedral site has more volume. We achieved this by using a 3-body term. Later Juslin and Nordlund produced a pair potential [9] that also reproduced this feature.
The total energy of the He–Fe system has the following form:

$$E = E_{Fe-Fe} + E_{He-He} + \sum_{\substack{i \in He \\ j \in Fe}} \phi\left(r_{ij}\right) + \sum_{\substack{i \in He \\ j,k \in Fe,\, j \neq k}} Y\left(r_{ij}, r_{ik}, \Theta_{jik}\right) \tag{1}$$

The iron interatomic potential E_{Fe-Fe} can be the pair potential by Finnis and Sinclair [10], the EAM potential by Ackland and Bacon [5] or the EAM potential by Ackland and Mendelev [11, 12]. The helium potential E_{He-He} is the one from Aziz [13]. The repulsive pair term ϕ is given by:

$$\phi\left(r_{ij}\right) = p_1 \exp\left(-p_4\left(\frac{r_{ij}}{p_3} - i\right)\right) f_{cut}\left(r_{ij}\right) \tag{2}$$

This function has a cutoff of 4.4Å. The 3-body term Y is given by:

$$Y\left(r_{ij}, r_{ik}, \Theta_{jik}\right) = \cos^2\left(\Theta_{jik} - 0.44\right) f_{cut}\left(r_{ij}\right) f_{cut}\left(r_{ik}\right) \tag{3}$$

This function has a cutoff of 2.2Å. The angle 0.44 radians is chosen so that the $\cos^2$ function has a minimum at the angle in the centre of a tetrahedron.

Simulation Method

The general procedure followed is:
• Generate perfect BCC lattice.
• Introduce the defect(s) to be studied.
• Relax at constant volume using a mixture of conjugate gradient and simulated annealing, and save the atom positions in units of the lattice constant.
• Start the MD simulation.
The MD simulation uses NVE dynamics. The lattice constant and initial velocities are chosen to give close to zero pressure and the desired initial temperature. The boundary conditions are periodic in *X*, *Y* and *Z*, which are ⟨100⟩ directions. The velocity Verlet algorithm with a timestep of 0.3fs is used. As volume and temperature correction are not used, when processes that release energy are simulated the temperature and pressure both rise during the simulation.

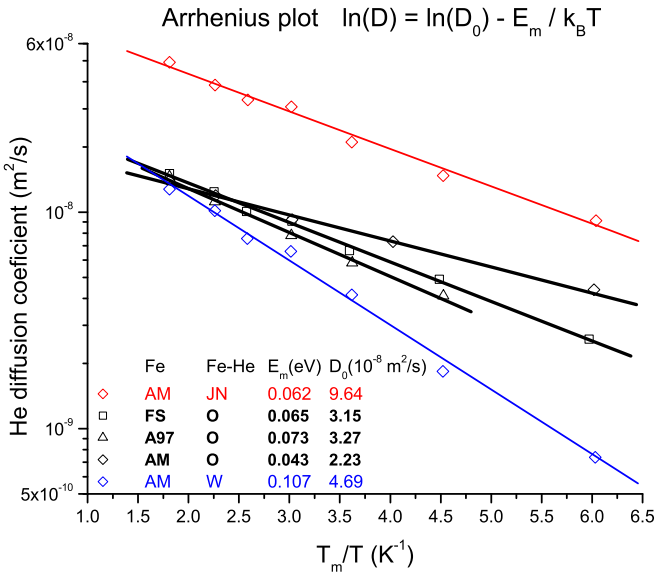

Figure 1. Arrhenius Plot for helium diffusion in iron matrix.

Single Helium Diffusion

Diffusion of an isolated interstitial He atom in a 10×10×10 BCC iron matrix (2,000 iron atoms) was simulated for several potentials at several temperatures. Arrhenius plots of the diffusion rates are shown in Fig. 1. The potentials used and fit parameters are shown in Table 1. The ORNL potential gives similar interstitial He migration barriers with three different iron matrices, all close to the 0.06eV value determined by DFT. The Juslin-Nordlund potential also gave a similar migration barrier, but much faster diffusion overall. The Wilson potential gave a higher barrier of 0.107eV. The diffusion rates are significantly more sensitive to the He-Fe potential used than to the iron matrix potential used.

Table 1. Migration barriers and diffusion rates of He in Fe for different potentials.

Symbol	Fe–Fe potential	Fe–He potential	E_m (eV)	D_0 ($10^{-8} m^2/s$)
◇	Ackland–Mendelev [11, 12]	Juslin–Nordlund [9]	0.062	9.64
□	Finnis–Sinclair [10]	ORNL [2–4]	0.065	3.15
△	Ackland–Bacon [5]	ORNL [2–4]	0.073	3.27
◇	Ackland–Mendelev [11, 12]	ORNL [2–4]	0.043	2.23
◇	Ackland–Mendelev [11, 12]	Wilson [6]	0.107	4.69

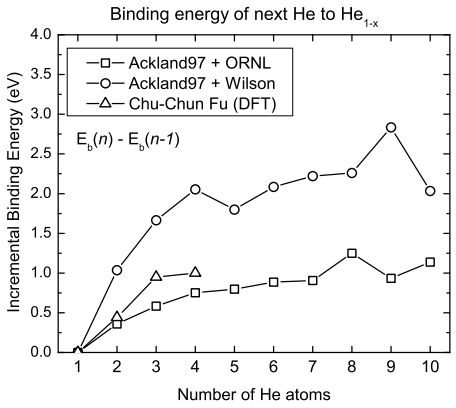

(a) He interstitial clusters

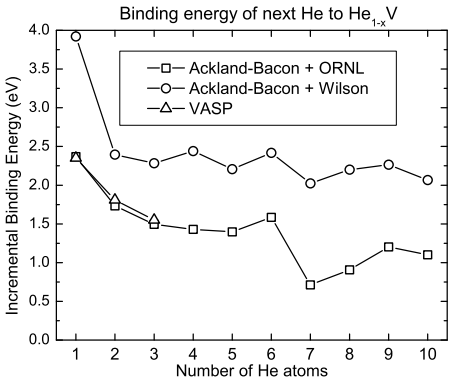

(b) Helium-Vacancy clusters

Figure 2. Cluster binding energies

Replacement Mechanism

Helium diffuses very fast in the matrix, but gets trapped in vacancies [14]. It is possible for a self-interstitial to recombine with the vacancy, kicking the helium into an interstitial position. To test whether this is favorable with this potential we performed static and dynamic calculations. Static calculations give formation energies for He_{sub}, He_{int} and SIA of 3.7, 4.3 and 4.9 eV respectively. Unsurprisingly $E(He_{sub}) + E(SIA) > E(He_{int})$, so recombination releases energy and is therefore favorable.

Static calculations for situations with more helium atoms are shown in Fig. 2. Figure 2a shows the incremental binding energy of an interstitial helium cluster as helium atoms are added. Figure 2b shows the incremental binding energy of a helium vacancy cluster as helium atoms are added. The simulations are done either in a 10×10×10 lattice or, for bigger defects, a 15×15×15 lattice (6,750 iron atoms). Calculations using both our He-Fe potential and Wilson's one are shown. *Ab initio* calculations by C.C. Fu and T. Seletskaia are also shown on the graphs for comparison. The ORNL potential results are closer to the *ab initio* results than are the Wilson potential ones.

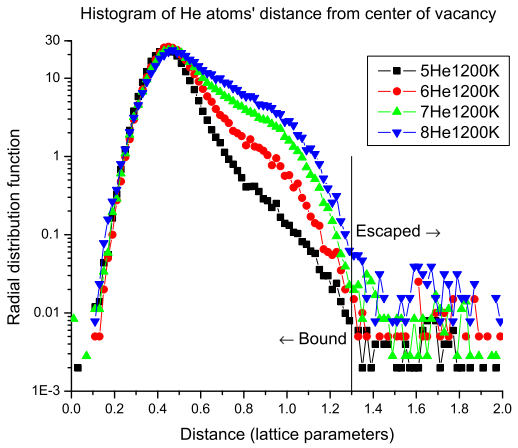

Figure 3. He atom location in HeV cluster

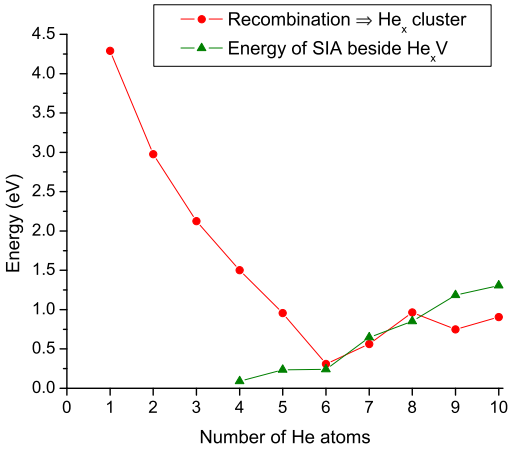

Figure 4. Energy differences for two processes

Dynamic simulations of helium-vacancy clusters are performed. The distribution of how far the He atoms are found from the centre of the vacancy is shown in Fig. 3. The most commonly observed configuration is an octahedron with the He atoms ~0.45 lattice parameters in the ⟨100⟩ directions, with any He atoms not part of the octahedron further out. As the helium is strongly bound to the vacancy, only results for 1200K are shown in order to observe helium atoms escaping within MD

timeframes. The results show that the helium atoms are bound out to a radius of 1.3 lattice parameters.

Dynamic simulations of an SIA and a helium-vacancy cluster at several temperatures are done to examine the replacement mechanism. Table 2 shows how many picoseconds it took for recombination to occur. As periodic boundary conditions and a small box were used, the SIA could not get away; if recombination is favorable it is likely to be observed in the simulation timeframe. For clusters with 5 or less helium atoms, recombination is observed at all temperatures tested. For He_6V, recombination is observed at 900K and 1200K but not at 600K, suggesting that recombination is favorable but has a high energy barrier to overcome. At 600K the SIA was trapped near the cluster but did not recombine. This was also observed for He_7V at both temperatures studied and for He_8V at 600K. For He_8V at 1200K a second SIA was ejected, creating an He_8V_2 cluster. The two SIAs were trapped next to it for 165ps, after which one of the SIAs recombined with the cluster, returning to the 1SIA + He_8V configuration.

Number of He atoms	300K	600K	900K	1200K
1	60.1	252.6	47.8	12.5
2		125.9		95.9
3		113.5		441.3
4	247.8	113.2		31.8
5	205.4	1363.6	320.7	35.4
6		didn't	4648.1	121.6
7		didn't		didn't
8		didn't		extra SIA

Table 2: Time in picoseconds for an SIA to recombine with a He_xV cluster

Using the results from Fig. 2, the amount of energy released when an SIA recombines with a He_xV cluster is calculated for different values of x and is plotted in Fig 4 (red circles). In some of the dynamic simulations an SIA was trapped close to a He-V cluster without recombining with it. Static calculations of this configuration are used to calculate the amount of energy released when an SIA moves into this position from far away. This is plotted as the green triangles in Fig. 4. If the vacancy contains 5 or less atoms, it is found to be energetically favorable for it to recombine with the SIA to form a helium interstitial cluster. For 6-8 atoms there is no clear winner, and for more than 8 it is more favorable for the SIA to be trapped nearby.

A dynamic simulation of a He_8 interstitial cluster at 600K showed that the reverse process can happen – an SIA was ejected, creating a He_8V cluster. The SIA was trapped beside the cluster.

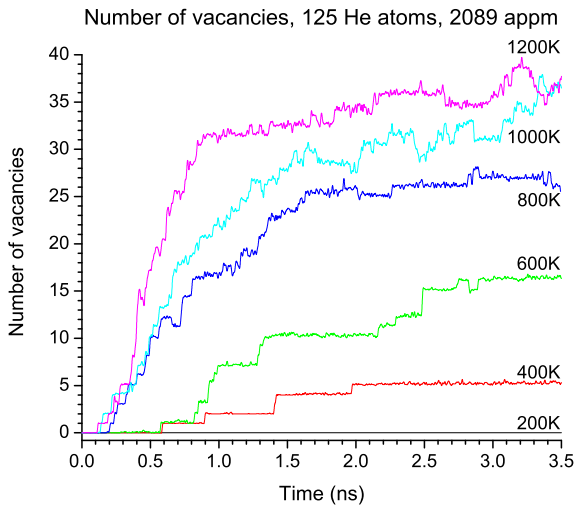

Figure 5. Vacancy production

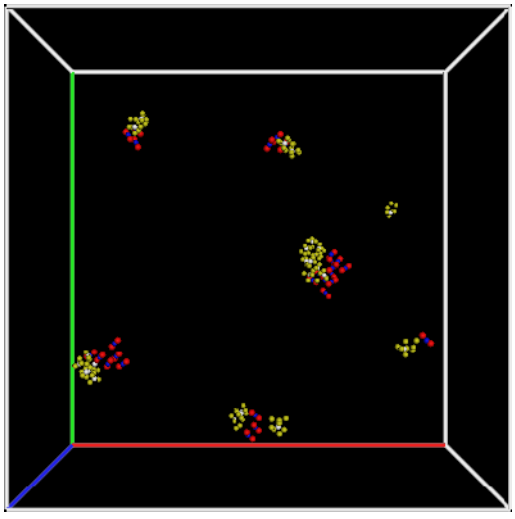

Figure 6. Clusters at 800K at t = 3.2ns

Coalescence

In order to see if helium interstitial clusters can form without a HeV + SIA recombination event, dynamic simulations were run with 125 helium atoms in a 31×31×31 BCC iron matrix (60,000 iron atoms). At 200K, there was insufficient kinetic energy to break up even a pair of He atoms, so the helium slowly and inexorably coalesced until it formed interstitial clusters too big to be mobile, He_4 or bigger. The largest observed cluster was He_7. No vacancies or SIAs were observed. At 400K, He_2 and He_3 were still mostly stable but more clusters were mobile so coalescence happened faster. When clusters reached 8 or 9 helium atoms, a single SIA was ejected. None of the ejected SIAs escaped their HeV cluster. At higher temperatures, smaller clusters like He_2 and He_3 were short lived, reducing the number of surviving clusters. The clusters that did form were bigger since the number of available He atoms was fixed at 125. The higher the temperature, the less He atoms were needed to eject an SIA. Higher temperatures also led to more SIAs escaping the HeV cluster where they were created. These SIAs were usually captured by other clusters that had SIAs. Groups of SIAs were observed to line up, forming dislocation loops.

The number of vacancies (equal to the number of SIAs ejected) is plotted as a function of time in Fig. 5. A snapshot of the 800K simulation after 3.2 nanoseconds is shown in Fig. 6. All the helium has coalesced into 9 clusters, all of which have pushed out from 1 to 6 SIAs. The SIAs have formed interstitial loops beside some of the clusters.

References

[1] S.I. Golubov, R.E. Stoller, S.J. Zinkle, and A.M. Ovcharenko, Kinetics of coarsening of helium bubbles during implantation and post-implantation annealing, Journal of Nuclear Materials 361 (2007), pp. 149–159.

[2] T. Seletskaia, Y. Osetsky, R.E. Stoller, and G.M. Stocks, Magnetic Interactions Influence the Properties of Helium Defects in Iron, Physical Review Letters 94 (2005), pp. 046403.

[3] T. Seletskaia, Y.N.Osetsky, R.E. Stoller, and G.M. Stocks, Calculation of helium defect clustering properties in iron using a multi-scale approach, Journal of Nuclear Materials 351 (2006), pp. 109–118.

[4] T. Seletskaia, Y.N. Osetskiy, R.E. Stoller, and G.M. Stocks, Development of a Fe He interatomic potential based on electronic structure calculations, Journal of Nuclear Materials 367 (2007), pp. 355–360.

[5] G.J. Ackland, D.J. Bacon, A.F. Calder, and T. Harry, Computer simulation of point defect properties in dilute Fe-Cu alloy using a many-body interatomic potential, Philosophical Magazine A-Physics Of Condensed Matter Structure Defects And Mechanical Properties 75 (1997), pp. 713–732.

[6] W. Wilson and R. Johnson, Rare Gases in Metals, Interatomic Potentials and Simulation of Lattice Defects, Battelle Institute Materials Science Colloquia, 1972, 375-390 (1972).

[7] C.C. Fu and F. Willaime, Ab initio study of helium in ®-Fe: Dissolution, migration, and clustering with vacancies, Physical Review B 72 (2005), pp. 064117.

[8] J.H. Evans, A. Van Veen, and L.M. Caspers, Direct Evidence for Helium Bubble Growth in Molybdenum by the Mechanism of Loop Punching, Scripta Metallurgica 15 (1981), pp. 323–326.

[9] K. Nordlund and S. Dudarev, Interatomic potentials for simulating radiation damage effects in metals, Comptes rendus-Physique (2008).

[10] M.W. Finnis and J.E. Sinclair, A simple empirical N-body potential for transition metals, Phil. Mag. A 50 (1984), pp. 45–55.

[11] M.I. Mendelev, S. Han, D.J. Srolovitz, G.J. Ackland, D.Y. Sun, and M. Asta, Development of new interatomic potentials appropriate for crystalline and liquid iron, Philosophical Magazine 83 (2003), pp. 3977–3994.

[12] G.J. Ackland, M.I. Mendelev, D.J. Srolovitz, S. Han, and A.V. Barashev, Development of an interatomic potentia for phosphorus impurities in agr-iron, Journal of Physics Condensed Matter 16 (2004), pp. 2629.

[13] R. Aziz, A. Janzen, and M. Moldover, Ab Initio Calculations for Helium: A Standard for Transport Property Measurements, Physical Review Letters 74 (1995), pp. 1586–1589.

[14] H. Trinkaus and B. Singh, Helium accumulation in metals during irradiation–where do we stand? Journal of Nuclear Materials 323 (2003), pp. 229–242.